USE OF DIGITAL IMAGE CORRELATION TO STUDY THE LOCAL DEFORMATION FIELD OF PAPER AND PAPERBOARD

J.M. Considine, C.T. Scott, R. Gleisner and J.Y. Zhu

USDA Forest Service, Forest Products Laboratory, Madison, Wisconsin

ABSTRACT

Digital image correlation was used to measure the full-field deformation of paperboard and handsheet tensile specimens. The correlation technique was able to accurately measure strain in regions 0.6 by 0.6 mm. Results showed the variation of strain to be much larger than has been previously reported. For machine-made paperboard tested in the cross-direction, the variation of strain increased throughout the tensile test and became erratic near failure, indicating many local failures. The measured strain distribution can be characterized by a Weibull function in agreement with weak-link failure theories. The analysis of a handsheet tensile specimen with a low-grammage region, approximately 4 mm wide, showed large negative strains near the region's edge.

INTRODUCTION

Paper scientists have long believed that formation affects paper behavior under stress. Moffat et al. [1] performed tensile tests on uncalendered newsprint and found that the failure zone passed through areas of below-average grammage. Lyne and Hazell [2] used holography to measure the deformation

field of paper during tension and found similar results to those of Moffat et al. [1]. Lyne and Hazell also found the correlation to be 0.81 between the Formation Index (Swedish Pulp and Paper Research Institute) and the CV(ε) (coefficient of variation, ε = strain). When strained at 90% of rupture, the maximum measured CV(ε) was 35%. Dodson [3] measured local strains in paper during tension and found the CV(ε) generally ranged from 20% to 30% using a microscope. Choi et al. [4] found that the CV(ε) in tensile paper specimens range from 23% to 40% during tensile testing using digital image analysis. These studies [2–4] demonstrated the CV(ε) was dependent on the scale of measurement.

Norman [5] recognized that separate factors were affecting paper tensile strength. Areas of low grammage reduced tensile strength and increased formation variability, whereas uniform formation increased tensile strength.

Ebeling [6] gave an important contribution to the understanding of the interaction of separate regions within a paper specimen under stress. He measured heat generation during the tensile straining of paper. Because heat adsorption increased during elastic tensile straining, he believed that load-carrying regions were increasing as the global stresses increased. Thus, the global strain was not homogeneous.

Perhaps the most exhaustive treatise on stochastic behavior of a fibrous network has been given on page 48 by Deng and Dotson [7]. Their network analysis provides an estimate of the variability of strain distribution.

$$\mathrm{CV}(\varepsilon) = \frac{\mathrm{CV(grammage)}}{1 + [\mathrm{CV(grammage)}]^2} \tag{1}$$

For most commercial papers, CV(grammage) ~ 10%, or less. By this estimate,

$$\mathrm{CV}(\varepsilon) < \mathrm{CV(grammage)} \tag{2}$$

Another important result of the Deng and Dodson [7] work was an analysis of inspection zone size as related to the measurement of the desired property. In particular, as the inspection zone size decreases, the CV of the desired property increases. Using a weak-link model of paper fracture, Hristopulos and Uesaka [8] showed the importance of the different scales of formation measurement and their relation to strength distribution of paper. Their results indicate that tensile strength is not well correlated to formation on a large scale (more than a few millimeters) but may be related to formation on a microscopic scale. In their analysis, the critical clusters—the "links" that carry most of the load—are less than 1 mm. Therefore, any deformation field

analysis for paperboard would need to be sensitive to displacements and distortions of regions less than 1 mm^2.

Several researchers have investigated the relationship between formation and strength. Korteoja et al. [9] found no relationship between the CV (grammage) and the CV (tensile strength) for two different machine-made papers. For each paper, the CV (tensile strength) was smaller in the CD (cross-machine direction) than the MD (machine direction). Nazhad et al. [10] showed that the effect of formation on tensile strength increases with increasing grammage in paper made from mechanical pulps. Mohlin [11] found no general correlation between formation and tensile strength for several machine-made papers. Clearly, the relationship between formation and strength depends on many variables such as fiber, pulping process, and fiber orientation and is stronger for some papers than others.

Strength, however, is only one property of interest. For packaging papers, modulus is a more critical property. Whereas many paperboard specifications include a strength requirement, it is usually important only during converting operations when the highest stress occurs for most uses of paperboard. However, failure of the final product can occur at much lower stress levels than those during converting. In corrugated containers, buckling occurs at a lower stress than does compressive failure. Buckling is strongly influenced by the state of local modulus. The local stress and strain states are directly related to the local modulus. Without direct measurement of local stress, the local modulus cannot be directly calculated but can be inferred only from local strain measurements. The local strain field of a paper specimen under tension has been experimentally measured with microscopes [3], interference holography [2], silicone impregnation [12], and digital image analysis [4], [13].

Korteoja et al. [12] examined the local strain field in paper by impregnating paperboard with a silicone gel and modeled that behavior with a computer simulation. The simulation showed that large portions of the specimen may not enter plastic deformation before rupture, which is similar to Ebeling's [6] conclusion regarding strain heterogeneity. The Korteoja et al. [12] computer model indicated that higher disorder (poorer formation) reduced the number of plastic yield sites. High strain concentrations at the plastic yield zone sites were sufficient to induce global failure before other regions of the specimen became plastic. Further evidence that local strains may be much larger than global strains is provided by Wathén et al. [14], who measured strains as high as 50% in a fracture process zone.

Korteoja et al. [15] used computer simulations to demonstrate how the CV(ε) changed during a tensile test. Their experimental and numerical model results showed that the rupture strain is more sensitive to local variations of

strain than the tensile strength. Furthermore, their model showed decreasing tensile strength and rupture strain with increasing formation-type variation and that

$$\mathrm{CV}(\varepsilon) \leq \mathrm{CV}(\text{modulus}) \tag{3}$$

Digital image correlation was used successfully by Um [13] to determine global elastic constants of paper and to examine the effect of holes in paper tensile specimens. His work showed the difficulty of numerically determining strain for the global deformation pattern. Wong et al. [16] used digital image correlation to confirm that local grammage and local strain are inversely proportional in uncalendared handsheets. This work focused on determining a failure criteria and recognized that strength relates to structure (formation) at a millimeter scale.

Our study evaluated the local deformation field of paperboard and handsheet specimens by direct observation. Images of specimens under increasing tension were captured and analyzed using digital image correlation. This study had two objectives: first, to determine the distribution of local strain during a tensile test and second, to demonstrate strain concentrations caused by poor formation.

MATERIALS

We used machine-made paper and prepared sets of handsheets for this study. The machine-made paper was a corrugating medium, nominally 126 g/m^2, made from NSSC hardwood pulp and incorporating approximately 30% recycled fiber.

A set of handsheets was formed with a nominal basis weight of 60 g/m^2 and a low-grammage region. The pulp used was commercially produced bleached kraft softwood at approximately 500 ml Canadian Standard Freeness. The handsheets were prepared according to the TAPPI-205 test method, with minor deviations described below.

For these handsheets, the standard backing wire below the 150-mesh forming screen was replaced with an 80-mesh screen. This screen was partially obstructed with four 6-mm-diameter plugs using hot-melt glue. The plugs were spaced approximately 20 mm apart near the center of the screen. This spacing allowed four 15-mm-wide test specimens to be cut from each handsheet, with the low-grammage region being located in the center of the test specimen. The obstructions limited the amount of fiber deposited in the region while maintaining “normal” formation on the rest of the sheet. The

low-grammage regions were approximately 0.03 mm thinner than the rest of the sheet, whose nominal caliper was 0.09 mm, using the method described by Setterholm [17].

Tensile testing and imaging

An Instron universal testing machine (Instron, Canton, Massachusetts) rotated to a horizontal position performed the tensile tests on the 15-mm-wide specimens, as illustrated in Figure 1. The crosshead speed was set at 10 mm per minute for the handsheets and 3 mm per minute for the machine-made paper while the gauge length of the clamps was set at 100 mm. The crosshead speed was lower for machine-made paper to compensate for the expected reduced failure strain. Load was measured with a Sensotec model 41 0–100-pound load cell (Honeywell-Sensotec, Columbus, Ohio), while cross head displacement was measured with a Hewlett-Packard 7DCDT linear variable differential transformer (Hewlett-Packard Co., Palo Alto, California). The load and displacement signals were collected on a computer using Measurement Computing data acquisition boards (Measurement Computing Corporation, Middlesboro, Massachusetts) and Labtech data logging

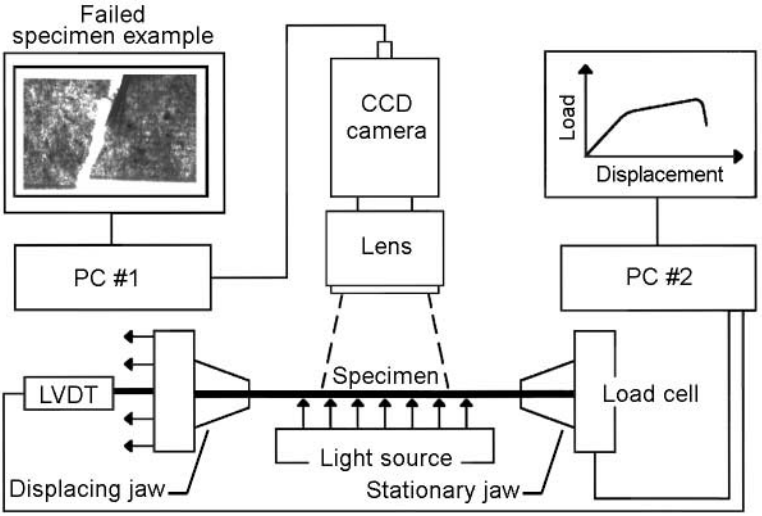

Figure 1 Schematic of image capture system. The LVDT is a Hewlett-Packard 7DCDT linear variable differential transformer. The camera contained a 640 by 480 charge-coupled device (CCD) array.

software (Labtech, Andover, Massachusetts). The signals were logged at 100 Hz. A 1-N preload was applied to the specimens to place them in the focal plane of the camera.

A Pulnix TM-6710 CL progressive scan camera (JAI Pulnix, Inc., Sunnyvale, California) was centrally mounted on a bracket above the Instron for capturing specimen images during a tensile test. A Navitar TV zoom lens (Navitar, Inc., Rochester, New York) was used on the camera and the shutter speed was set to 0.001 s. The camera contained a 640 by 480 CCD (charge-coupled device) array. Images were captured at 120 Hz by a Coreco PC Cam-link frame grabber (Coreco Imaging, Billerica, Massachusetts). Sherlock Essential machine vision software (IPD, Billerica, Massachusetts) logged the images. Because of the high image collection rate, it was necessary to temporarily log the images to random access memory using RamDisk XP software provided by Cenatek (Cenatek, Inc., Morgan Hill, California). A typical handsheet tensile test would last 20 to 25 s and would require up to 0.9 gigabytes of memory.

A portion of the specimen was illuminated by a Dolan-Jenner uniform diffuse fiber optic backlight (Dolan-Jenner Industries, Lawrence, Massacusetts). The 25- by 40-mm backlight was mounted 0.5 mm below the test specimen and centrally located between the grips.

Image analysis

In this experiment, the inherent paper features enhanced by transmitted light were used for image correlation. To eliminate the possibility of reducing local strain variation, random patterns were not applied even though correlation may have been enhanced.

The images were analyzed by a Matlab toolbox, MatPIV [18], which is free and has open source code. MatPIV was designed to use digital image correlation for particle image velocimetry in fluids. A thorough description of digital image correlation is given in Sveen [18]. Digital image correlation relies on pattern matching and compares two images by dividing each image into smaller interrogation windows, and using matrix correlation of the interrogation windows, determines the relative movement of the interrogation window in one image with respect to the other image. In our case, the first image, I_1, captured was the reference image and each subsequent image, I_n, where n is the image number, $n > 1$, was compared to the reference image. The relative movement of an interrogation window in I_n is determined by shifting the interrogation window throughout I_1. The location of the interrogation window in I_1 that gives the highest 2-D correlation is compared to its location in I_n. The difference in locations is the relative movement. Sub-pixel dis-

placements are calculated by using a 3-point Gaussian curve fit to determine the 'real' peak of the correlation.

In this experiment, four different windows sizes were used: 128 by 128, 64 by 64, 32 by 32, and 16 by 16 pixels. For the analysis, each image was subdivided into the specified window size, such as 64 by 64 pixels, and was correlated with the reference image taken at the beginning of the test. The result was a displacement map of the deformed image compared to the reference image. In some cases, the deformations were so large that a 16 by 16 pixel window could not be well correlated between the images. The smaller window, 16 by 16 pixels, had less data to correlate than a 32 by 32 pixel window. When large amounts of distortion occurred within a 16 by 16 pixel region, the region had many poor correlations with several regions in I_1 and the calculated displacement had significant error. The distortion became progressively worse throughout the test until the interrogation window did not correlate reliably with any region in I_1.

The conversion from pixel displacement to actual displacement was determined by using a calibration image of dots arranged in a rectangular pattern of 4.7 dot/mm. A 16- by 16-pixel window corresponded to a 0.6- by 0.6-mm area and was smaller than the critical cluster size suggested by Hristopulus and Uesaka [8].

The image analysis procedure provided a u (x-direction) and v (y-direction) displacement field for the entire viewing area. Recall the strain-displacement relations

$$\begin{aligned} \varepsilon_x &= \partial u/\partial x \\ \varepsilon_y &= \partial v/\partial y \\ \gamma_{xy} &= \partial u/\partial y + \partial v/\partial x \end{aligned} \tag{4}$$

where ε_x, ε_y, are the normal strains in the x, y directions and γ_{xy} is the shear strain.

In this report, all strains were calculated using four-point central finite difference formula, except where noted. For any function $f(z)$ then

$$f'(z)_0 = (-f_2 + 8f_1 - 8f_{-1} + f_{-2})/(12h) + \text{higher order terms}$$

where f_i = value of $f(z)$ at point i

h = distance between points, assumes equal spacing between points.

Or in terms of displacement, the strain in the x-direction at point 0 is

$$\varepsilon_{x,0} = (-u_2 + 8u_1 - 8u_{-1} + u_{-2})/(12h) \tag{5}$$

RESULTS

This section contains results for specific specimens that were representative for this study.

The output of the digital image correlation routine was a group of arrays containing u, v displacements for the positions x, y on the specimen. Equation (5) was used to calculate an ε_x array from the u and x arrays. The ε_x array was the local strain, based on window size, for each window position in the x, y arrays. The mean of the ε_x array is the macroscale ε_x for the captured image. For the system shown in Figure 1, the displacement was negative based on the origin location at the lower left corner of the viewing area.

Figure 2 shows an example displacement contour of a specimen at 7.0 s after test initiation. The window size was 32 by 32 pixels and corresponded to an area of 0.6 by 0.6 mm for this lens magnification. The mean slope of the displacement contour is the global strain for this specimen-viewing area. Each interrogation window is identified by the grid on the displacement contour.

Figure 3 shows a representative strain calculation for the midline of a paperboard specimen aligned in the CD under tension at 38.3 s. For this specimen, failure occurred at 74.7 s. The line represents the discrete data points determined from image analysis. Each marker represents the strain as

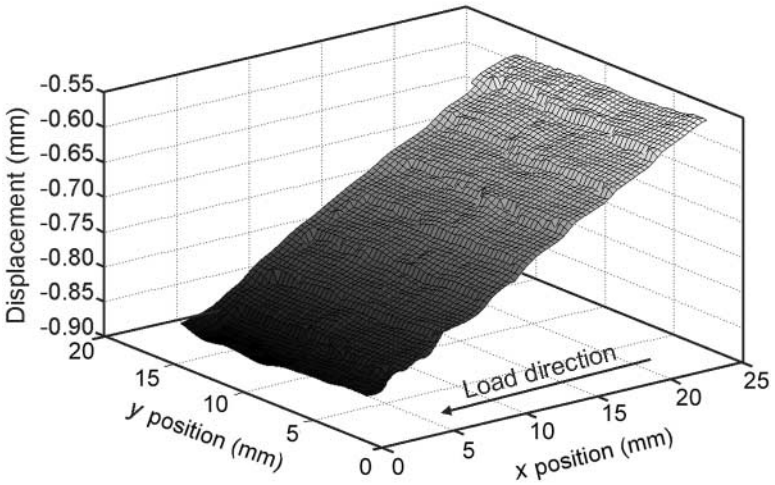

Figure 2 Displacement contour for handsheet specimen 7.0 s after test initiation.

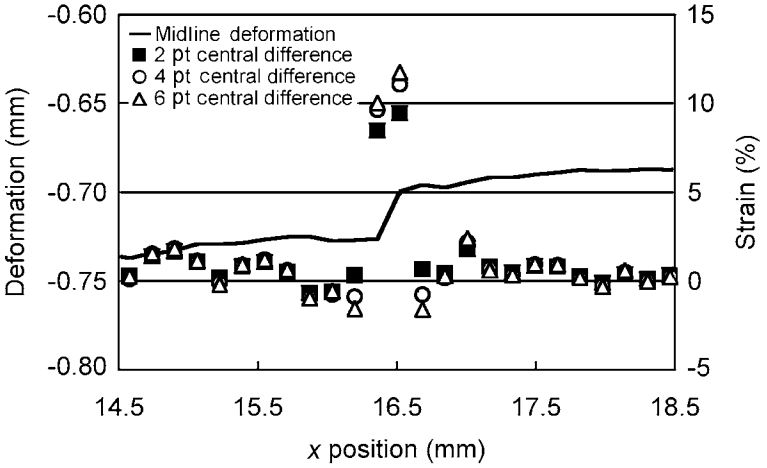

Figure 3 Strain calculation for the midline of a paperboard specimen.

determined by three different finite difference formulas. To examine the relationships given in Equations (2) and (3), this study focused on estimating the variation of microscale strain in the specimen caused by formation. We did not use a numerical smoothing technique because this technique would be more applicable for the measurement of macroscale strain. Our study used a finite difference calculation of strain (Equation (5)) to determine the local variation of strain.

Table 1 provides the statistical analysis for ε_x on a complete line; a portion of the line was shown in Figure 3. The strain determined by jaw displacement is the global strain of the specimen. Precise agreement of the calculated strain with the global strain is not expected because the calculated strain is only measured on approximated 25% of the specimen. The slope of the regression

Table 1 Strain Calculation Information

Strain calculation method	Mean strain	
Jaw displacement	2.0%	
Regression	2.3%	$R^2 = 97.4\%$
Two-point central difference	2.2%	$CV(\varepsilon_x) = 131\%$
Four-point central difference	2.2%	$CV(\varepsilon_x) = 157\%$
Six-point central difference	2.2%	$CV(\varepsilon_x) = 170\%$

of the deformation line is the average strain across the camera-viewing area. We expected the large CV(ε_x) for each finite difference calculation. We will show later that the distribution of the strain changes dramatically as the test progresses. The general agreement of global strain and mean strain, as determined by image correlation, was consistent for all specimens in this study and provided confidence that the errors in strain measurement were small.

Figure 4 compares the mean ε_x for two different window sizes with the global strain. The analysis was from the same specimen as Figure 3. The strain as measured by grip displacement is denoted "Instron." The remaining strain calculations are based on different size pixel windows. In this case, a 16-by 16-pixel window represents a region 0.6 by 0.6 mm. This test lasted 74.7 s. The first part of the analysis used the initial image for each window size (taken at 0 s) as the reference image until 42.9 s. From 42.9 to 74.7 s, the strain analysis for each window size used the image captured at 42.9 s. The mean ε_x calculation—the average of all the window strains in the specimen at a particular time—agrees reasonably well with that determined from the grip displacement. We expected large strain, as calculated by digital image correlation, near the end of the test because this specimen failed within view of the camera. When the specimen failed within the captured image, the calculated

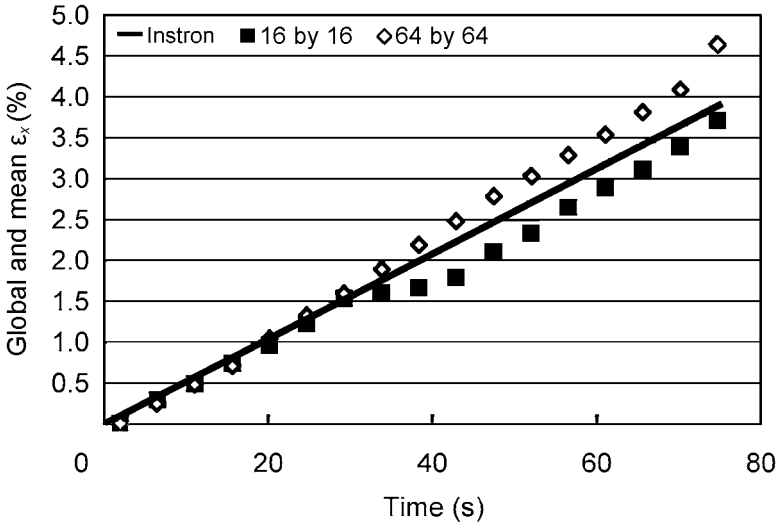

Figure 4 Global ε_x comparison for two window sizes.

mean ε_x was larger than the global ε_x because of the extremely high strains within the rupture region. The general similarity between the mean ε_x calculated by a 16- by 16-pixel window size and the grip displacement was important because researchers [8] investigating formation have suggested the "critical element" in paper is approximately 1 mm^2. From the load-time information, we know that at 30 s, the specimen transitions from homogeneous to heterogeneous strain behavior. The differences in mean strain between the 16- by 16-pixel and the 64- by 64-pixels windows were caused by the narrow width of the rupture line. The narrow width reduced the number of 16- by 16-pixel windows with high strain.

Figure 5 shows the effect of window size on the determination of the standard deviation of ε_x within the specimen. The specimen was machine-made paperboard and tested in the CD. The y-axis scale was chosen to show the differences between window sizes. As a result, some of the 16- by 16-pixel data were not included in this figure. This particular specimen was chosen for two reasons. First, while the standard deviations of strain were increasing throughout the test, the 16- by 16-pixel window was no longer able to correlate with the reference image after about 36 s. However, the larger examination windows were able to correlate with the reference image up to failure. When

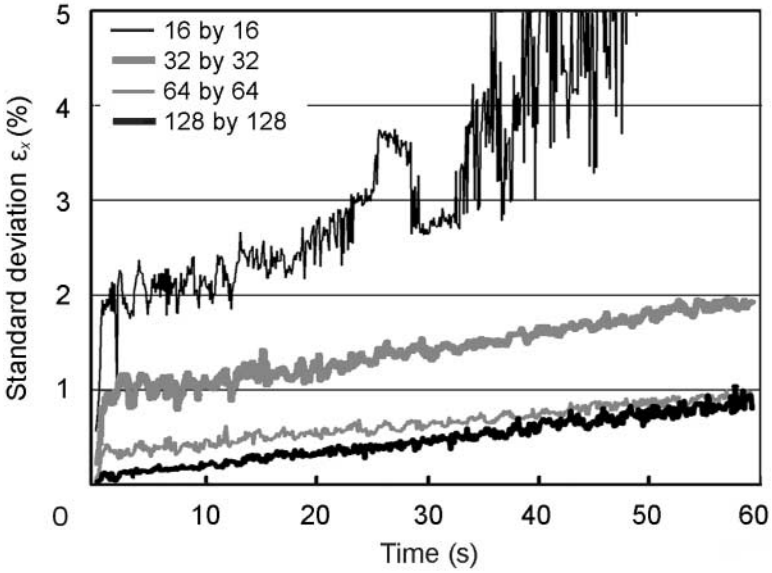

Figure 5 Effect of window size on standard deviation of ε_x.

the length of a side of the examination window is halved, the area of the window is reduced by a factor of four, and we might expect the variability of an average window property to quadruple. This would lead to a doubling of the standard deviation of the property. For lower image numbers, a doubling of strain standard deviation with a halving of window side length appears to hold at least approximately. For example, at 13 s the standard deviations are 0.21%, 0.46%, 1.21%, and 2.66% for sides of length 128, 64, 32, and 16 pixels.

The definition of engineering strain is applicable to a continuum, even at a microscale. When a region experienced local failure, the areas near the local failure experienced very high strain and redistributed the stresses. Once a local failure has occurred, the engineering definition of strain becomes problematic. From the point of view of the image correlation process, a local failure produced a new feature not present in the reference image. If enough features remained near the local failure, then the image correlation continued. If not, then the analysis began to fail, as shown in Figure 5 for the 16- by 16-pixel window size, when the standard deviation became erratic.

As a tensile test progresses, more and more regions within the specimen experience plastic deformation and local failure. The CD tests showed a large amount of variation of strain, presumably because the MD-oriented fibers change shape to distribute the stress. One measure of the local failure is the variation of strain within the specimen and is illustrated in Figure 6. While the specimen data in Figure 5 showed increasing variation of ε_x throughout the test, the specimen in Figure 6 began to indicate a large amount of local failures well before global failure, as shown by the erratic CV(ε_x) near the end of the test. The strain was calculated by digital image correlation using a 32- by 32-pixel window size and a four-point central finite difference.

The magnitude of CV(ε_x) was larger than the 20% to 40% previously measured [2–4] and is a result of the smaller region of investigation. In Figure 6, near failure, CV(ε_x) was greater than 400%. According to Equation (3), which has been used by [7] and [15], the CV(modulus) is same order of magnitude as CV(ε_x). Most paper researchers consider the CV(modulus) < 10% for ordinary papers and paperboards. Our results suggest more investigation of the relationship between CV(ε_x) and CV(modulus) is required. At about 50 s, the CV(ε_x) increases dramatically and becomes erratic even while the mean ε_x remains smooth.

Figure 7 shows the microscale ε_x for a machine-made paperboard near failure. The reference image was 4.1 s before the final image prior to failure. The ε_x shows the strain at $x = 5$ mm to be approximately 5%, when the global strain was 0.2% for that time period. This specimen ruptured along the line $x = 5$ mm, where the strain peak is shown in Figure 7. Approximately 25% of the total deformation of the 100-mm specimen occurred within 1 mm. Of

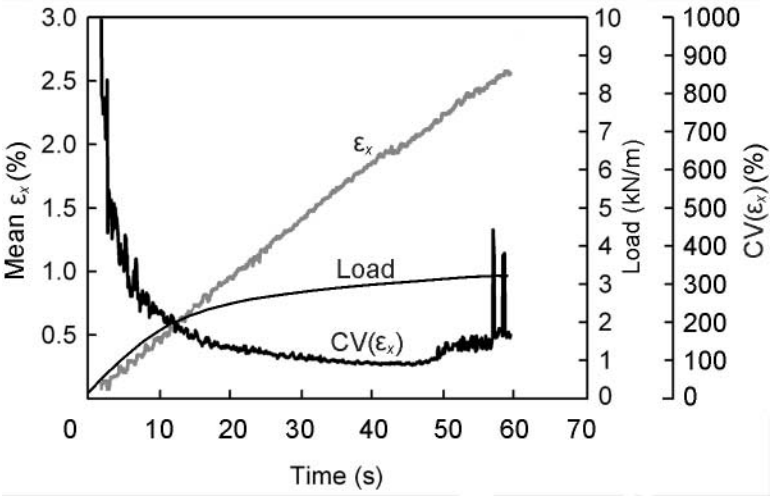

Figure 6 Erratic behavior of CV(ε_x) near specimen failure, even while mean ε_x remains smooth, indicates local failures are occurring.

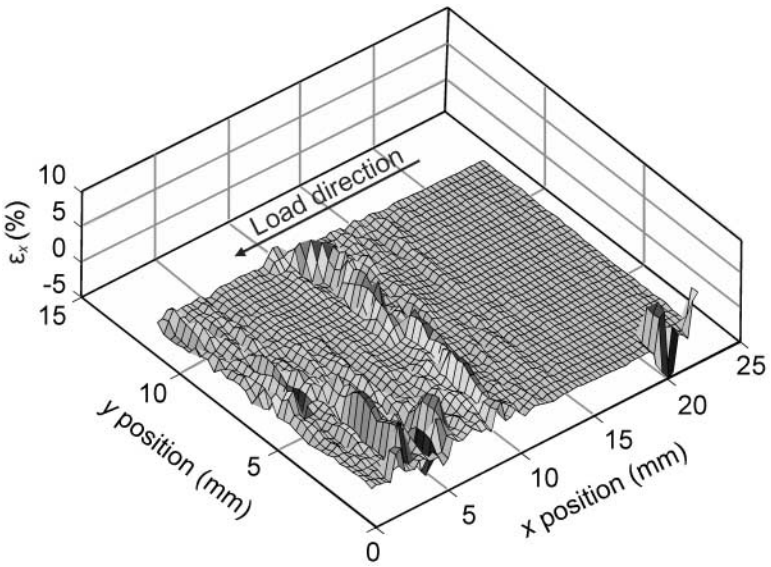

Figure 7 ε_x contour near failure zone.

course, the strain for this period is in addition to the strain prior to the reference image.

As the specimen is stressed, the shape of the ε_x distribution within the specimen changes, as shown in Figure 8a,b. The data are from handsheet specimens without the low-grammage region. The data for each time (5.0,

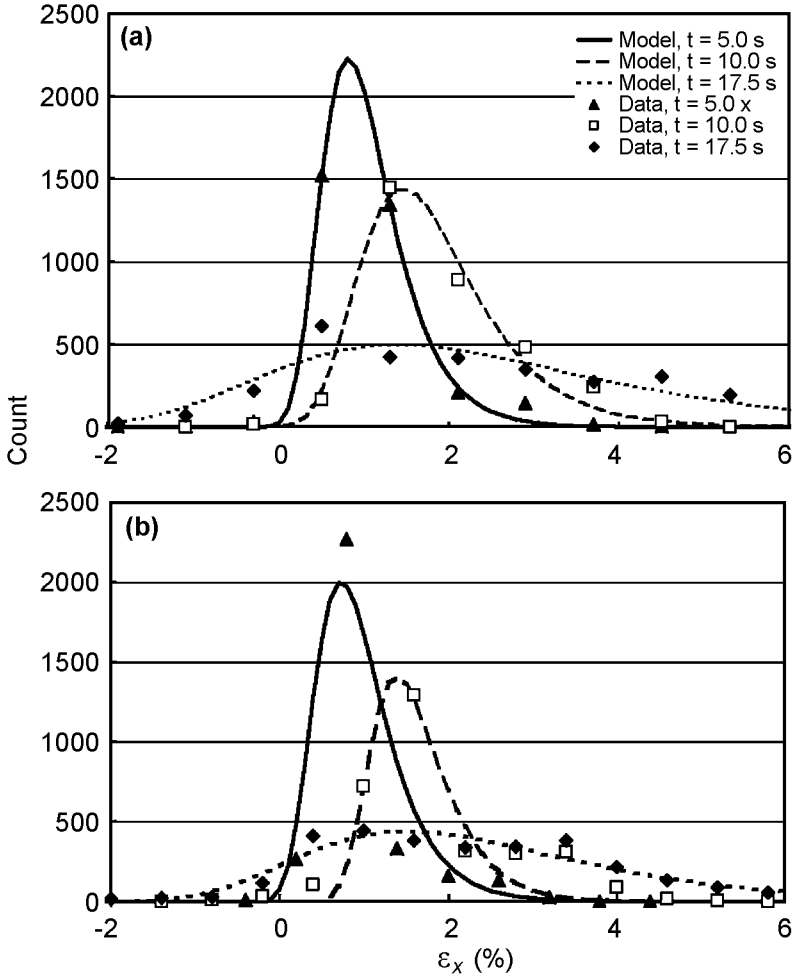

Figure 8 Strain histograms of two samples at different times during tensile straining. Data was fit to a 3-parameter Weibull distribution.

10.0, and 17.5 s) was fit to a 3-parameter Weibull distribution. This Weibull distribution has been used to model weak-link fracture [8]. An isotropic material would be represented by a single line, centered on the mean strain, gradually moving to the right during the test. Early in each test, the strain was almost homogeneous, but as the test progressed, local failures occurred and stress was redistributed to other regions, causing heterogeneous strain. Near the end of the test, many local failures had occurred and some regions "snapped back" to zero strain or less. Some regions had initial residual tensile stress that was released during local failures. These failures caused the analysis method to calculate negative strain. In this case, negative strain is *not* necessarily compressive strain. The portion of the distribution less than 0% strain was greater for $t = 17.5$ s than for $t = 10.0$ s. Furthermore, as modeled by [12], a number of regions had strains larger than 10%.

The difficulty in measuring the effect of formation on paper is largely a problem of the test material. No two researchers are able to prepare paper samples with "exactly" the same properties because of the variable nature of paper and paperboard. Researchers have examined the effect of formation [8–11] and defects [19] on the strength of paper and paperboard. As stated earlier, some researchers have concluded that no correlation exists between current formation measurements and strength, whereas others have measured some relationship between formation and strength.

Paper physicists hypothesize that a relationship should exist between formation and strength. We have developed a crude system of making areas of low grammage in a handsheet mold so that specimens with similar formation features could be reproduced. This method was described earlier. Figure 9 shows an example of an image with a low-grammage region within a tensile specimen. The image was the reference image used for this particular specimen. The low-grammage region was approximately 4 mm along the x-direction, the direction of straining. This size region was chosen for several reasons: first, it is obvious within the handsheet, it is easy to reproduce, and finally, we fundamentally understand the stress behavior during tension for a low-modulus region in an infinite sheet.

Figure 10 shows two lines of deformation across the length of the specimen at a time near failure. In this graph, the low-grammage region existed from 8 to 12 mm along the x-direction. At this particular time, the deformation line across the top of the low-grammage region had two areas of high strain, just less than 8 and just more than 12 mm. The deformation line through the center of the region had a very high *negative* strain area around 13 mm. In this case, the negative strain *is* compressive strain. One of the reasons to use a low-grammage region was to demonstrate this circumstance. This negative strain region is predicted by a classical mechanics analysis of a low-modulus

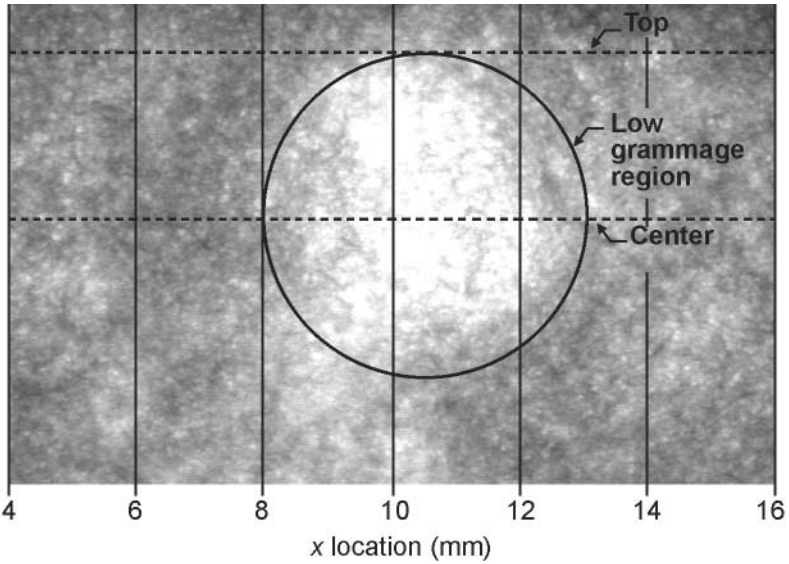

Figure 9 Grey-scale image of a low-grammage region within a tensile specimen. Data from the top and center of region in the image were used to calculate Figure 10.

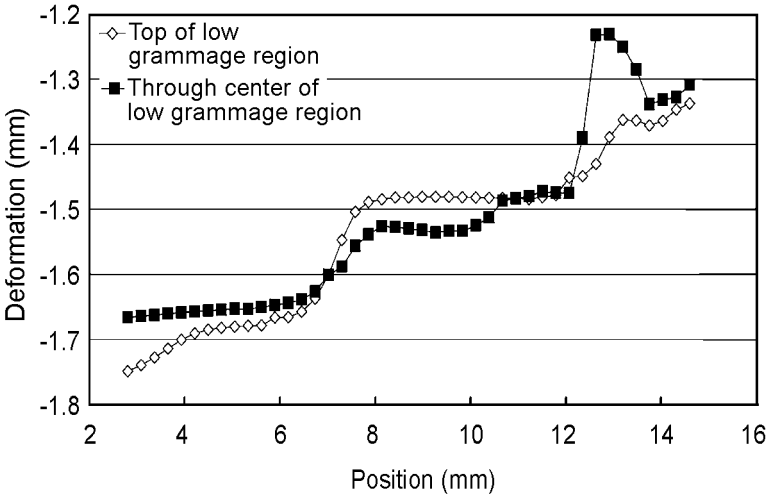

Figure 10 Two lines of deformation across length of specimen at time near failure. These lines were calculated from the image data in Figure 9.

region in an infinite plate under uniform tension. Paper has a much lower strength in compression than tension, so by this example, a "poor" formation exists that can significantly reduce strength. The formation can be so "poor" that local compressive stresses are created even during global tensile stresses.

CONCLUSIONS

- Digital image correlation can be an effective technique to examine local strain behavior of fibrous networks under stress.
- The variation of strain increases during straining as regions undergo plastic deformation and failure. In most cases, the variation of strain is a precursor to failure.
- The variation of strain measured by digital image correlation is much higher than previously reported. One reason for this larger variation is that digital image correlation uses smaller regions than those used in previous studies. Also, this technique determined strains from an entire region within the specimen, and not just selected regions.
- The distribution of strains changes as the global stress level increases. The shape can be characterized by a Weibull distribution in agreement with weak-link failure theories.
- Regions of low grammage were shown to have the characteristic shape and size required to produce compressive stresses during tensile testing in agreement with classical mechanics.

REFERENCES

1. Moffatt, J.M., L.R. Beath, and W.G. Mihelich. Major Factors Governing Newsprint Strength. in *The Fundamental Properties of Paper Related to its Uses, Transactions of the 5th Fundamental Research Symposium*. 1973: First published 1976 by Ernest Benn Limited, 25 New Street Square, London, EC4A VA & Sovereign Way, Tonbridge, Kent, TN9 IRW for the Technical Division of the British Paper and Board Industry Federation Plough Place, Fetter Lane, London, EC4A I AL.
2. Lyne, M.B. and R. Hazell. Formation Testing as a Means of Monitoring Strength Uniformity. in *The Fundamental Properties of Paper Related to its Uses, Transactions of the 5th Fundamental Research Symposium*. 1973: First published 1976 by Ernest Benn Limited, 25 New Street Square, London, EC4A VA, & Sovereign Way, Tonbridge, Kent, TN9 IRW for the Technical Division of the British Paper and Board Industry Federation Plough Place, Fetter Lane, London, EC4A I AL.
3. Dodson, C.T.J. *A Contribution to the Development of a Statistical Rheology of Bonded Fibrous Networks*. Brunel University, 1968.

4. Choi, D., J.L. Thorpe, and R.B. Hanna. *Image analysis to measure strain in wood and paper*. Wood Sci. Technol. **25**:251–262, 1991.
5. R.J. Norman. Dependence of sheet properties on formation and forming variables. In Consolidation of the Paper Web, *Trans. IIIrd Fund. Res. Symp. Cambridge, 1965*, (F. Bolam, ed.), pp. 269–298 FRC, Manchester, 2003. ISBN: 0 9541126 3 6.
6. Ebeling, K. *Distribution of Energy Consumption During the Straining of Paper*. in *The Fundamental Properties of Paper Related to its Uses, Transactions of the 5th Fundamental Research Symposium*. 1973: First published 1976 by Ernest Benn Limited 25 New Street Square, London, EC4A VA & Sovereign Way, Tonbridge, Kent, TN9 IRW for the Technical Division of the British Paper and Board Industry Federation, Plough Place, Fetter Lane, London, EC4A I AL.
7. Deng, M. and C.T.J. Dodson. p. 284 in **Paper – An Engineered Stochastic Structure.** Tappi, Atlanta, GA, 1994.
8. Hristopulos, D.T. and T. Uesaka. Factors that Control the Tensile Strength Distribution in Paper. in *2003 International Paper Physics Conference*. 2003. Victoria, BC, Canada: Pulp and Paper Technical Association of Canada, Montreal, Canada.
9. Korteoja, M., et al. Statistical variation of paper strength. *Journal of Pulp and Paper Science*. **24**(1):1–7, 1998.
10. Nazhad, M.M., et al. The influence of formation on tensile strength of papers made from mechanical pulps. *Tappi J.*, **83**(12):63, 2000.
11. Mohlin, U.B. Fiber dimensions: formation and strength. *Nord. Pulp Pap. Res. J*, **16**(3):235–239, 2001.
12. Korteoja, M.J., et al. Local strain fields in paper. *Tappi J.* **79**(4):217–223, 1996.
13. Um, G.J., Experimental Investigation on the Mechanical Properties of Paper Material Using Image Correlation Analysis. p. 206 in *College of Environmental Science and Forestry*. Syracuse University, Syracuse, New York, 2003.
14. Wathén, R., et al. Determining the critical strain in the fracture process zone by different methods. in *2003 International Paper Physics Conference*. Victoria, BC, Cananda: Pulp and Paper Technical Association of Canada, Montreal, Canada. 2003.
15. Korteoja, M.J., et al. Computational study of formation effects on paper strength. J. Pulp and Paper Science, 1997. **23**(1): p. J18–J22.
16. Wong, L., M.T. Kortschot and C.T.J. Dodson. *Effect of Formation on Local Strain Fields and Fracture of Paper. J. Pulp Pap. Sci.* **22**(6):J213–219, 1996.
17. Setterholm, V.C. Dimensional Property Measurements. pp 403–414. in *Handbook of Physical and Mechanical Testing of Paper and Paperboard* (eds. R.E. Mark and K. Murakami), Marcel Dekker, New York, NY, 1984.
18. Sveen, J.K. An introduction to MatPIV v. 1.6.1. in *Mechanics and Applied Mathematics*. Dept. of Math, University of Oslo, Oslo, Norway, 2004.
19. Koskinen, T., M. Kosonen, and K. Ebeling. The impact of paper defects on paper strength requirements, in *The science of papermaking, 12th Fundamental research symposium*. Oxford, UK, Bury, UK, The Pulp and Paper Fundamental Research Society, 2001.